LETTERS

Kinematic variables and water transport control the formation and location of arc volcanoes

T. L. Grove[1], C. B. Till[1], E. Lev[1], N. Chatterjee[1] & E. Médard[1]†

The processes that give rise to arc magmas at convergent plate margins have long been a subject of scientific research and debate[1–6]. A consensus has developed that the mantle wedge overlying the subducting slab[3,4] and fluids and/or melts from the subducting slab itself[6–11] are involved in the melting process. However, the role of kinematic variables such as slab dip and convergence rate in the formation of arc magmas is still unclear. The depth to the top of the subducting slab beneath volcanic arcs, usually ~110 ± 20 km, was previously thought to be constant among arcs[3,6,12]. Recent studies[13,14] revealed that the depth of intermediate-depth earthquakes underneath volcanic arcs, presumably marking the slab–wedge interface, varies systematically between ~60 and 173 km and correlates with slab dip and convergence rate. Water-rich magmas (over 4–6 wt% H_2O) are found in subduction zones with very different subduction parameters, including those with a shallow-dipping slab (north Japan), or steeply dipping slab (Marianas). Here we propose a simple model to address how kinematic parameters of plate subduction relate to the location of mantle melting at subduction zones. We demonstrate that the location of arc volcanoes is controlled by a combination of conditions: melting in the wedge is induced at the overlap of regions in the wedge that are hotter than the melting curve (solidus) of vapour-saturated peridotite and regions where hydrous minerals both in the wedge and in the subducting slab break down. These two limits for melt generation, when combined with the kinematic parameters of slab dip and convergence rate, provide independent constraints on the thermal structure of the wedge and accurately predict the location of mantle wedge melting and the position of arc volcanoes.

The extent and maximum depth of hydrous melting at subduction zones are controlled by the supply of water from the subducting slab to the overlying mantle wedge. New experimental work[15,16] shows that chlorite, $[Mg_{4.6}Fe_{0.3}Cr_{0.1}Al][Si_3Al]O_{10}(OH)_8$, which contains 13 wt% water, is stable in the mantle wedge to depths of 100–120 km. As water is released from the slab at shallow depths, it rises into overlying mantle and hydrates it through the formation of chlorite. This chlorite zone is advected to depth by corner flow as the sinking slab drags overlying mantle downward. This zone of chlorite stability in the wedge dehydrates at temperatures slightly above the vapour-saturated solidus. Water released from chlorite breakdown is then transferred

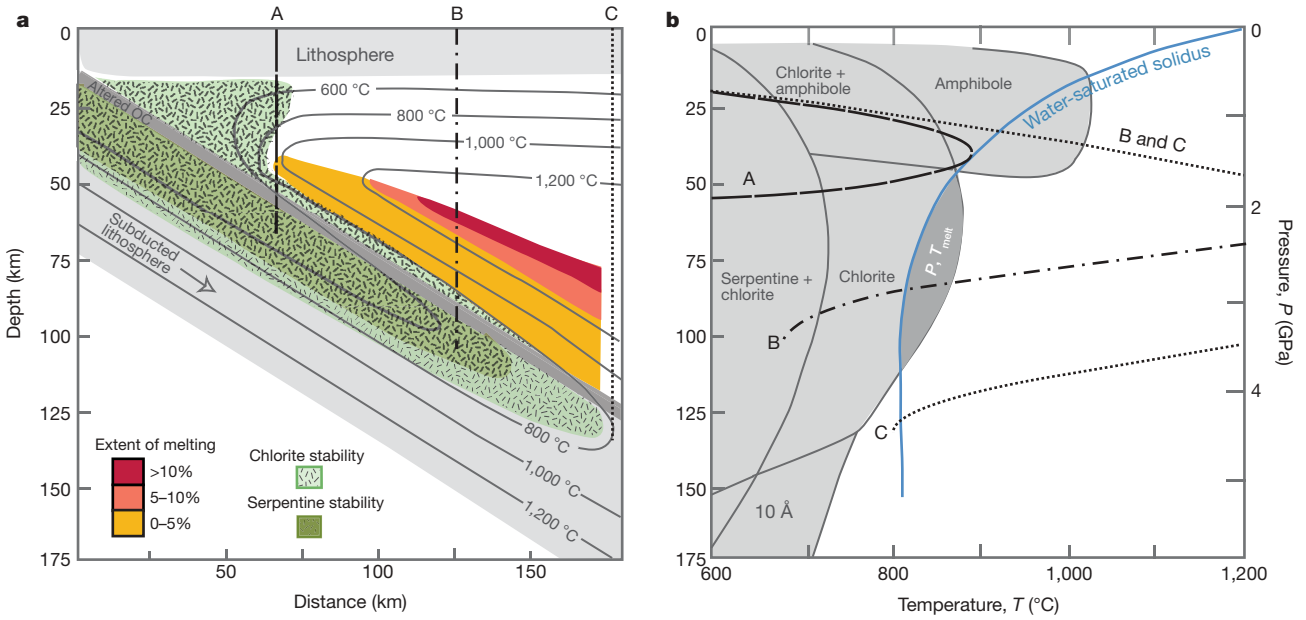

Figure 1 | Diagrams showing limits for melt generation. **a**, A typical subduction zone with melting model (after ref. 15) using our thermal model with a dip of 30° and a convergence rate of 40 mm yr^{-1}, and depicting the hydrous phase (>10 wt% water) stability fields within the subducted lithosphere and mantle wedge[15,16,18–22]. **b**, Hydrous peridotite phase diagram. In **a**, the vertical lines A, B and C denote vertical cross-sections through the mantle wedge and in **b** they denote a path through a pressure–temperature phase diagram for vapour-saturated peridotite. The dark-grey region in **b** labelled 'P, T_{melt}' indicates the pressure–temperature region required for melting in our geodynamic models.

[1]Department of Earth, Atmospheric and Planetary Sciences, Massachusetts Institute of Technology, Cambridge, Massachusetts 02139, USA. †Present address: Laboratoire Magmas et Volcans, Université Blaise Pascal, Clermont-Ferrand, F-63038, France.

into a vapour-saturated melt (Fig. 1). The temperature of chlorite breakdown is ~200 °C hotter than temperature estimates of the slab–wedge interface for hot slab subduction[17,18]. Therefore, the presence of chlorite in the wedge provides a mechanism for transporting significant quantities of water (up to 2 wt% H_2O in bulk peridotite) into the mantle[19] even in hot subduction zones and removes the need for dry melting in hot slab environments, as has been proposed for some subduction zones[9].

The maximum depth stability of hydrous minerals, and thus the maximum depth water released within the slab can ascend into the overlying mantle wedge, is influenced by the temperature structure in the subducted lithosphere (Fig. 1). Serpentine and the 10 Å phase are two hydrous minerals, in addition to chlorite, that are stable to considerable depths in the subducted oceanic lithosphere[18–21] (up to 150 km, depending on the pressure–temperature structure of the slab). Amphibole was once proposed as a carrier for transporting water to depth in the mantle[4,5], but amphibole becomes unstable at depths shallower than the depths at which melting begins beneath most arc volcanoes. As shown in the new vapour-saturated peridotite melting experiments[15,16,22], amphibole is stable from ~0.8 to 2 GPa on the solidus and chlorite is stable from 2 to 3.6 GPa (ref. 16; Fig. 1b).

Here we incorporate these new observations regarding the stability of hydrous minerals and the vapour-saturated peridotite solidus to estimate the effect of kinematic subduction parameters on the distribution of flux melting in subduction zones. Many studies indicate that convergence rate and the dip of the downgoing slab at subduction zones probably strongly affect the location of arc volcanoes at convergent margins[13,14,23–25]. The convergence rate influences the advection of heat by corner flow in the mantle wedge and the diffusion of heat across the steep temperature gradient induced between the cold slab and the hot upper mantle[5,13,26–29]. Slab dip determines the geometry of the flow of hot mantle into the wedge corner. To isolate and constrain the effects of slab dip and convergence rate on the location and size of the melting region at convergent margins, we construct a set of geodynamic models.

We construct two-dimensional finite-element models of kinematically driven subduction following the set-up defined in the subduction community benchmark model[30]. Slab dips in our model span the range found for most subduction zones and vary between 32° and 64°. In the same way, we vary slab velocities from 20 to 100 mm yr^{-1}. For each combination of parameters, we calculate the steady-state thermal structure of the slab and wedge. Mantle rheology in our models is Newtonian, isotropic and temperature-dependent, as is appropriate for the upper mantle. Grid resolution is 2.3 km in both the vertical and horizontal directions.

After finding the thermal structure of the slab and the mantle wedge, we calculate the region of potential melting by comparing the stability regions of chlorite and the vapour-saturated solidus of peridotite[15,16]. When water ascends by porous flow into the hotter, shallower parts of the mantle wedge, melting begins at a critical distance from the trench where temperature first exceeds that of the vapour-saturated solidus (Fig. 1, path A). Fluid ascent paths closer to the wedge corner never reach temperatures that exceed the vapour-saturated solidus (Fig. 1, to the left of path A). Between paths A and C in Fig. 1, melting may occur by one of two mechanisms (Fig. 1, path B). If a water-rich fluid is present, melting will begin at the vapour-saturated solidus. If there is no free fluid phase, chlorite breakdown, at a temperature slightly above the vapour-saturated solidus, will initiate melting. In our models, we have chosen the region of melting to be above the vapour-saturated solidus but below the chlorite breakdown reaction between 2 and 3.6 GPa (~60 and 110 km depth, respectively) (region labelled 'P, T_{melt}' in Fig. 1b). Above 3.6 GPa (~110 km), little to no melting will occur because the water necessary for vapour-saturated melting is not present (Fig. 1, path C) as the upper-temperature limit for hydrous phase stability plunges below the vapour-saturated solidus. (At pressures below 2 GPa, vapour-saturated melting might be possible if

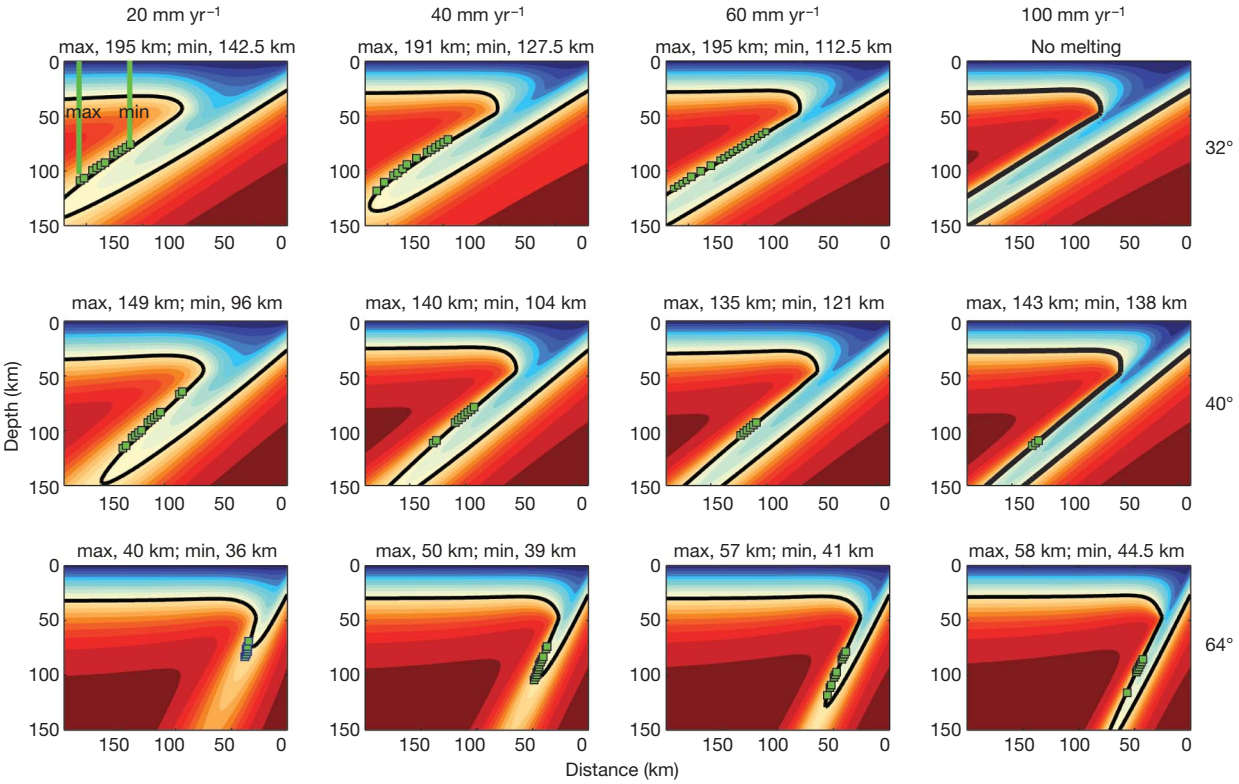

Figure 2 | Thermal structure of the mantle wedge and subducting slabs calculated from finite-element modelling and the location of the initiation of vapour-saturated melting. Rows have constant slab dip (in degrees) and columns have constant slab velocity (convergence rate in mm yr^{-1}). Green squares denote the initiation of hydrous melting by marking elements above the temperature of the vapour-saturated peridotite solidus and within the chlorite stability field (region labelled 'P, T_{melt}' in Fig. 2). The thick black contour follows the 800 °C isotherm. The values above each plot state the minimum and maximum distances (in kilometres) of melting from the trench (defined in top left plot).

Table 1 | Outputs from our geodynamic models with measured arc volcano locations

Arc name	Convergence rate (km per million years)	Slab dip (degrees)	Depth to slab (km)	Arc–trench distance (km)
Central Aleutians	60	58	183 (ref. 14); 44 (ref. 13)	90 (ref. 14); 90 (ref. 13)
Model similar to the central Aleutians	60	64	40	80
New Zealand	36	50	96 (ref. 14); 92 (ref. 13)	123 (ref. 14); 110 (ref. 13)
Model similar to New Zealand	40	40	104	70

Data for modern subduction zones from ref. 13 did not contain direct measurements of distance from trench to arc. We calculate this value from their measurements of depth to slab and the slab dip by a simple geometric approximation: (depth to slab)/tan (slab dip).

the mantle wedge temperature exceeds the vapour-saturated solidus. We have chosen not to examine this process in our model.)

The thermal structures resulting from the range of slab dips and convergence rates we examine are depicted in Fig. 2. Our modelling results suggest the dip of the slab is an order of magnitude more important than the convergence rate in controlling the location of the isotherms in the mantle at subduction zones. As the slab steepens, hotter mantle can reach shallower depths in the mantle wedge corner (Fig. 2), leading to larger extents of melting. Additionally, slab dip has a first-order effect on the total width of the melting region: shallower slabs lead to wider melting regions, suggesting a correlation between slab dip and arc width. Jarrard[12] and Tatsumi[6] noted a similar relationship between slab dip and arc width. Tatsumi attributed it to the dehydration of hydrous minerals in the subducting lithosphere. Our model and experiments indicate that this correlation results from chlorite dehydration and melting in the mantle wedge.

Our models reveal a clear relationship between slab dip and the position of the melting region, a relationship we confirm by observations from subduction zones worldwide. For steeply dipping slabs, the melting region is closer to the trench and the surface width of the melting region (that is, the width of the volcanic arc) is narrower than for shallow-dipping slabs (Fig. 2). A plot of the distance from the trench to the volcanic arc front (which we assume to lie directly above the edge of the melting region) as a function of the sine of the slab dip reveals a clear linear trend with a negative correlation. Observations from arcs worldwide, collected by England *et al.*[13] and Syracuse and Abers[14] confirm this linear negative correlation between trench–arc distance and the sine of slab dip that we find in our models (Fig. 3). The slope

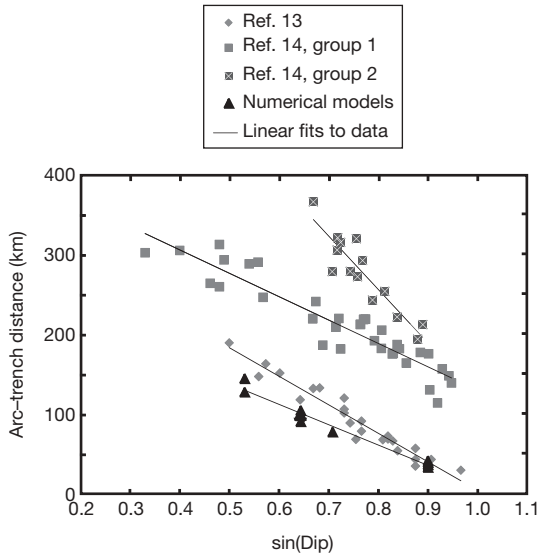

Figure 3 | Distance between the arc front and trench versus the sine of slab dip for subduction zones worldwide and for our numerical models. Models (shown as triangles) follow the same trend as the data of ref. 13 and those from South and Central America in ref. 14 ('group 1'). Data from Alaska and the western Pacific in ref. 14 ('group 2') follow a second, steeper trend. The constant offset of ~100 km between the ref. 14 'group 1' data and the data from ref. 13 are explained by the different techniques used to estimate the trench position. Solid lines are linear fits to the data.

from our models is similar to the slopes obtained from refs 13 and 14. This agreement demonstrates a fundamental relationship between slab dip and the location of melting and arc volcanism. Interestingly, part of the data set of ref. 14 ('group 2') shows a secondary steeper linear trend, which has yet to be explained.

The correlation between convergence rate and the location of the melting region or melt productivity is less clear. In general, there is no systematic influence of convergence rate on the width of the melting region (Fig. 2). At a dip of 32°, the melting region systematically widens with increasing convergence rate, whereas at a dip of 40°, the melting region narrows.

Predictions of the location of melting from our geodynamic models for subduction zones correspond well with the locations of the central Aleutian and New Zealand arcs. In Table 1, the locations of volcanic front for the central Aleutian and New Zealand arcs are compared to geodynamic models we constructed with similar kinematic variables. In both cases, our models predict results within 10 km of the observed locations of arc volcanoes, suggesting our model is a good first-order approximation of the effect of kinematic variables on the thermal structure of the mantle wedge and the location of melting at subduction zones.

In conclusion, the petrologic control on mantle melting at subduction zones is the temperature of the vapour-saturated peridotite solidus and the supply of water to the mantle wedge from the breakdown hydrous minerals, predominantly chlorite in the mantle wedge and subducted lithosphere. The kinematic control on the location of mantle melting is primarily slab dip and, to a lesser degree, the convergence rate. Thus, regions of the mantle wedge saturated with fluid and above the temperature of the vapour-saturated peridotite solidus will melt, and the size and location of this melting region will vary linearly with slab dip. Our experimental work and models adequately explain worldwide observations regarding the location of arc volcanoes and clarify the effect of the kinematic variables, such as slab dip and convergence rate, on the formation of arc magmas.

Received 11 February; accepted 6 April 2009.

1. Toksoz, M., Minear, J. & Julian, B. Temperature field and geophysical effects of a downgoing slab. *J. Geophys. Res.* **76,** 1113–1138 (1971).
2. Ringwood, A. The petrological evolution of island arc systems. *J. Geol. Soc.* **130,** 183–204 (1975).
3. Gill, J. B. *Orogenic Andesites and Plate Tectonics* 390 (Springer, New York, 1981).
4. Wyllie, P. Subduction products according to experimental prediction. *Geol. Soc. Am.* **93,** 468–476 (1982).
5. Davies, J. H. & Stevenson, D. J. Physical model of source region of subduction zone volcanics. *J. Geophys. Res.* **97,** 2037–2070 (1992).
6. Tatsumi, Y. The subduction factory: how it operates in the evolving Earth. *GSA Today* **15,** 4–10 (2005).
7. Moran, A. E., Sisson, V. B. & Leeman, W. P. Boron depletion during progressive metamorphism—implications for subduction processes. *Earth Planet. Sci. Lett.* **111,** 331–349 (1992).
8. Yogodzinski, G. M., Kay, R. W., Volynets, O. N., Koloskov, A. V. & Kay, S. M. Magnesian andesite in the western Aleutian Komandorsky region - implications for slab melting and processes in the mantle wedge. *Geol. Soc. Am.* **107,** 505–519 (1995).
9. Stern, C. R. & Kilian, R. Role of the subducted slab, mantle wedge and continental crust in the generation of adakites from the Andean Austral volcanic zone. *Contrib. Mineral. Petrol.* **123,** 263–281 (1996).
10. Kelemen, P. B., Hart, S. R. & Bernstein, S. Silica enrichment in the continental upper mantle via melt/rock reaction. *Earth Planet. Sci. Lett.* **164,** 387–406 (1998).
11. Plank, T. & Langmuir, C. H. Tracing trace-elements from sediment input to volcanic output at subduction zones. *Nature* **362,** 739–743 (1993).

12. Jarrard, R. D. Relations among subduction parameters. *Rev. Geophys.* **24,** 217–284 (1986).
13. England, P., Engdahl, R. & Thatcher, W. Systematic variation in the depths of slabs beneath arc volcanoes. *Geophys. J. Int.* **156,** 377–408 (2004).
14. Syracuse, E. M. & Abers, G. A. Global compilation of variations in slab depth beneath arc volcanoes and implications. *Geochem. Geophys. Geosyst.* **7,** Q05017, doi:10.1029/2005GC001045 (2006).
15. Grove, T. L., Chatterjee, N., Parman, S. W. & Medard, E. The influence of H_2O on mantle wedge melting. *Earth Planet. Sci. Lett.* **249,** 74–89 (2006).
16. Till, C. B., Grove, T. L., Withers, A. C. & Hirschmann, M. M. Extending the wet mantle solidus: implications for H_2O transport and subduction zone melting processes. *AGU Fall Meet. Suppl.* Abstract D142A–02 (2007).
17. Kelemen, P. B., Rilling, J. L., Parmentier, E. M., Mehl, L. & Hacker, B. R. in *Inside the Subduction Factory* (ed. Eiler, J. M.) 293–311 (American Geophysical Union, 2003).
18. Pawley, A. Chlorite stability in mantle peridotite: the reaction clinochlore plus enstatite=forsterite+pyrope+H_2O. *Contrib. Mineral. Petrol.* **144,** 449–456 (2003).
19. Iwamori, H. Transportation of H_2O and melting in subduction zones. *Earth Planet. Sci. Lett.* **160,** 65–80 (1998).
20. Schmidt, M. W. & Poli, S. Experimentally based water budgets for dehydrating slabs and consequences for arc magma generation. *Earth Planet. Sci. Lett.* **163,** 361–379 (1998).
21. Fumagalli, P. & Poli, S. Experimentally determined phase relations in hydrous peridotites to 6.5 GPa and their consequences on the dynamics of subduction zones. *J. Petrol.* **46,** 555–578 (2005).
22. Medard, E. & Grove, T. L. Early hydrous melting and degassing of the Martian interior. *J. Geophys. Res.* **111,** E1103 (2006).
23. Kincaid, C. & Sacks, I. S. Thermal and dynamical evolution of the upper mantle in subduction zones. *J. Geophys. Res.* **102,** 12295–12315 (1997).
24. van Keken, P. E., Kiefer, B. & Peacock, S. M. High-resolution models of subduction zones: implications for mineral dehydration reactions and the transport of water into the deep mantle. *Geochem. Geophys. Geosyst.* **3,** doi:10.1029/2001GC000256 (2002).
25. England, P. & Wilkins, C. A simple analytical approximation to temperature structure in subduction zones. *Geophys. J. Int.* **159,** 1138–1154 (2004).
26. Peacock, S. M., Rushmer, T. & Thompson, A. B. Partial melting of subducting oceanic-crust. *Earth Planet. Sci. Lett.* **121,** 227–244 (1994).
27. Kirby, S. H., Durham, W. B. & Stern, L. A. Mantle phase-changes and deep-earthquake faulting in subducting lithosphere. *Science* **252,** 216–225 (1991).
28. Molnar, P. & England, P. Temperatures, heat-flux, and frictional stress near major thrust faults. *J. Geophys. Res.* **95,** 4833–4856 (1990).
29. McKenzie, D. Speculations on the consequences and causes of plate motions. *Geophys. J. R. Astron. Soc.* **18,** 1–32 (1969).
30. van Keken, P. E. *et al.* A community benchmark for subduction zone modeling. *Phys. Earth Planet. Inter.* **171,** 187–197 (2008).

Acknowledgements We thank the reviewers for their constructive comments. This research was supported by the NSF.

Author Contributions T.L.G., C.B.T., N.C. and E.M. participated in the experimental study that led to the phase diagram for water-saturated peridotite melting. T.L.G. and C.B.T. formulated the hypothesis presented in the paper. E.L. carried out the geodynamic modeling. All authors participated in the writing and revision of the paper.

Author Information Reprints and permissions information is available at www.nature.com/reprints. Correspondence and requests for materials should be addressed to T.L.G. (tlgrove@mit.edu).